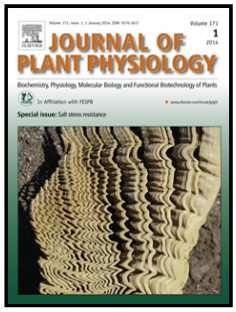

Title: The dynamics and endocytosis of Flot1 protein in response to flg22 in *Arabidopsis*

Authors: Meng Yu, Haijiao Liu, Ziyi Dong, Jianwei Xiao, Bodan Su, Lusheng Fan, George Komis, Jozef Šamaj, Jinxing Lin, Ruili Li

PII: S0176-1617(17)30130-X
DOI: http://dx.doi.org/doi:10.1016/j.jplph.2017.05.010
Reference: JPLPH 52584

To appear in:

Received date: 22-2-2017
Revised date: 16-5-2017
Accepted date: 16-5-2017

Please cite this article as: Yu Meng, Liu Haijiao, Dong Ziyi, Xiao Jianwei, Su Bodan, Fan Lusheng, Komis George, Šamaj Jozef, Lin Jinxing, Li Ruili.The dynamics and endocytosis of Flot1 protein in response to flg22 in Arabidopsis.*Journal of Plant Physiology* http://dx.doi.org/10.1016/j.jplph.2017.05.010

The dynamics and endocytosis of Flot1 protein in response to flg22 in *Arabidopsis*

Meng Yu[1,4], Haijiao Liu[1,4], Ziyi Dong[1], Jianwei Xiao[1], Bodan Su[1], Lusheng Fan[2], George Komis[3], Jozef Šamaj[3], Jinxing Lin[1] and Ruili Li[1,*]

[1]College of Biological Sciences and Technology, Beijing Forestry University, Beijing 100083, China

[2]Department of Botany and Plant Sciences, University of California, Riverside, CA 92521, USA

[3]Centre of the Region Hana for Biotechnological and Agricultural Research, Faculty of Science, Palacky University, 78301 Olomouc, Czech Republic

[4]These authors contributed equally to this article.

*Corresponding author: Dr. Ruili Li, College of Biological Sciences and Biotechnology, Beijing Forestry University, Qinghua East Road 35, Beijing 100083 China, Email: liruili@bjfu.edu.cn

ABSTRACT

Membrane microdomains play vital roles in the process of bacterial infection. The membrane microdomain-associated protein Flot1 acts in an endocytic pathway and is required for seedling development, however, whether Flot1 is a part of host defense mechanisms remains unknown. During an analysis of callose deposition, we found that Flot1 amiRNAi mutants exhibited defects in response to flg22. Using variable-angle total internal reflection fluorescence microscopy (VA-TIRFM), structured illumination microscopy (SIM) and fluorescence cross spectroscopy (FCS), we determined that the dynamic behavior of GFP-Flot1 in *Arabidopsis thaliana* cotyledon epidermal cells changed significantly in plants treated with the elicitor flg22. Moreover, we found that Flot1 was constitutively recycled via an endocytic pathway and that flg22 could promote endocytosis. Importantly, targeting of Flot1 to the late endosome/vacuole for degradation increased in response to flg22 treatment; immunoblot analysis showed that when triggered by flg22, GFP-Flot1 was gradually degraded in a time-dependent manner. Taken together, these findings support the hypothesis that the changing of dynamics and oligomeric states can promote the endocytosis and degradation of Flot1 under flg22 treatment in plant cells.

Key words Flot1, dynamics, endocytosis, VA-TIRFM, SIM

1. Introduction

Membrane microdomains are sterol- and sphingolipid-rich nano-scale domains within the plasma membrane. These highly dynamic domains contain glycosylphosphatidylinositol (GPI)-anchored proteins and a subset of integral and peripheral cell surface proteins (Simons and Toomre, 2000). Substantial evidence supports a regulatory role for membrane microdomains in signal transduction, membrane trafficking, organization of the actin cytoskeleton, and the response to pathogen attack (Lajoie and Nabi, 2010; Liu et al., 2009; Ovečka et al., 2010; Simons and Gerl, 2010). Proteomic analyses of the detergent-resistant membrane (DRM)

fraction of plant extracts have mainly been performed in tobacco (*Nicotiana tabacum*), *Arabidopsis thaliana* and *Medicago truncatula* (Borner et al., 2005; Morel et al., 2006; Kierszniowska et al., 2009). These studies identified important proteins involved in signaling, cellular trafficking, responses to biotic/abiotic stress, and cell wall metabolism (Morel et al., 2006; Lefebvre et al., 2007; Keinath et al., 2010). For example, respiratory burst oxidase homolog (RbohD) (Morel et al., 2006; Fujiwara et al., 2009; Kierszniowska et al., 2009) and Feronia (Keinath et al., 2010) are enriched in DRMs. Lipid metabolism associated enzymes such as phospholipase D (PLD), phospholipase C (PLC), and PIP2-specific PLC were also detected in DRMs (Shahollari et al., 2004; Kierszniowska et al., 2009; Keinath et al., 2010).

Membrane microdomains play vital roles in plant immune signaling (Simon-Plas et al., 2011). Shortly after flg22 treatment, several proteins, such as FLS2, H^+ ATPase, sugar transporters, Ca^{2+}-dependent kinases, and syntaxin, relocalize to DRMs (Keinath et al., 2010). Elicitation with the fungal elicitor cryptogein triggers a decrease in the association of dynamin-related proteins with DRMs in tobacco cells (Stanislas et al., 2009). StREM1.3, one of Remorin family proteins, can directly interact with the movement protein TRIPLE GENE BLOCK PROTEIN1 to interfere with cell to cell movement of *Potato Virus* X (PVX) (Raffaele et al., 2009; Perraki et al., 2012). Remorin also forms clusters on the plasma membrane at the bacterial infection site during nodule symbiosis of *Medicago truncatula* to monitor bacterial signaling molecules in the host–bacterial interaction (Lefebvre et al., 2010). Flotillins, which are used as membrane microdomain markers in mammalian and plant cells (Glebov et al., 2006; Li et al., 2012), are required for the symbiosis between the nitrogen-fixing bacterium *Sinorhizobium meliloti* and its host, the legume *Medicago truncatula* (Haney and Long, 2010). Haney and Long (2010) identified seven genes encoding flotillin-like (FLOT) proteins in *Medicago truncatula* and showed that *FLOT2* and *FLOT4* are strongly upregulated during early symbiotic events. Furthermore, an increase in Lysin motif receptor-like kinase3 (LYK3) and FLOT4-mCherry colocalization was observed in symbiont-inoculated root hairs (Haney and Long, 2010; Haney et al., 2011). More interestingly, Flotillins play

important roles in pathogen defense, such as *Dictyostelium* resistant to *Mycobacterium marinum* infection, *Chlamydia pneumoniae* growth in A549 epithelial cell lines and Litopenaeus vannamei resistant to white spot syndrome virus infection (Hagedorn and Soldati, 2007; Korhonen et al., 2012; Shi et al., 2016).

Defining the endocytosis and trafficking pathways of cell surface proteins in plants is an important step in establishing the function of these proteins. For example, PIN-FORMED (PIN) proteins enter cells through the action of clathrin-dependent endocytosis and localize to the *trans*-Golgi/early endosomal compartments. PIN proteins are recycled back to the plasma membrane via a Brefeldin A-sensitive pathway, or localized to the vacuole for degradation, resulting in their polar localization (Geldner et al., 2001; Geldner et al., 2003; Kleine-Vehn and Friml, 2008). AtFlot1 localizes to membrane microdomains and is involved in clathrin-independent endocytosis (Li et al., 2012). However, the mechanisms underlying the endocytosis and vesicle trafficking of Flot1 remain largely unknown.

In this study, we used variable-angle total internal reflection fluorescence microscopy (VA-TIRFM) and structured illumination microscopy (SIM) (Komis et al., 2015a, b; Li et al., 2011; Wan et al., 2011) to reveal that the velocity of Flot1-GFP increased and then Flot1-GFP aggregated in PM by treated with flg22.Furthermore, we also found that flg22 can promote Flot1-GFP endocytosis. Most importantly, Flot1 protein was gradually degraded in a time-dependent manner after treatment with the flg22 elicitor. The results of this study provide valuable information for further investigation of the regulatory mechanisms of membrane microdomains in the plant defense response.

2. Materials and methods

2.1. Plant materials and growth conditions

All experiments were performed using *Arabidopsis thaliana* ecotype Columbia-0 (Col-0). *Flot1* amiRNA knockdown lines were developed in our laboratory (Li et al.,

2012). Transgenic *Arabidopsis thaliana* seeds expressing VHA-a1-mRFP and RabG3f-mRFP were described previously (Zhang et al., 2011). Seeds were surface sterilized in 70% ethanol for 2 minutes, transferred to 5% (w/v) NaClO for 15 min, washed with distilled water at least five times, and plated on half-strength Murashige and Skoog (MS) medium (1/2x MS) containing 1% (w/v) sucrose and 0.8% (w/v) agar (Duchefa, The Netherlands), followed by stratification at 4°C in the dark for 2 d. The plants were grown under 16 h light/8 h dark conditions at 20–22°C.

2.2. Plasmid construction and plant transformation

The 35S:: GFP-Flot1 construct was produced as described previously (Li et al., 2012). Double-labeled transgenic plants containing GFP-Flot1/VHA-a1-mRFP, GFP-Flot1/RabG3f-mRFP and GFP-Flot1/SNX1-mRFP were generated by crossing plants harboring the following constructs: GFP-Flot1 with VHA-a1-GFP, RabG3f-mRFP and SNX1-mRFP.

2.3. Semi-quantitative RT-PCR

Total RNA was extracted from WT and amiRNAi15-1, 15-5, 30-2, and 32-1 *Arabidopsis* seedlings using Trizol according to the manufacturer's protocol (Invitrogen). Reverse transcription was performed using a First-Strand cDNA Synthesis kit (Invitrogen) and an oligo (dT) primer. For semi-quantitative RT-PCR, *Flot1* was amplified via 28 cycles of PCR using specific primers (Table S1); the *ACTIN2* (AT3G18780) gene used as an internal control. All experiments were performed at least three times.

2.4. Analysis of callose deposition

Aniline blue staining was performed to analyze flg22-induced callose deposition as described previously (Kim et al., 2005). Briefly, seven-day-old seedlings grown in solid 1/2 MS medium were transferred to liquid 1/2 MS medium containing 10 μM flg22 for 24 h. The seedlings were then washed twice in ethanol : acetic acid(1:3[v/v]) for 20 h and stained for 24 h with 0.01% aniline blue in 150 mM KH_2PO4 (pH 9.5). Callose was visualized in cotyledons by epifluorescence microscopy.

2.5. Yeast two-hybrid analysis

Gal4-based yeast two-hybrid assays were performed using the Matchmaker Gold Yeast Two-Hybrid System from Clontech according to the manufacturer's instructions. The vectors pGADT7 and pGBKT7 were used to construct the prey and bait plasmids, respectively. The primers used for plasmid construction for the yeast assays are listed in supporting information Table S2. Y2H Gold yeast cells containing each of the activation domain constructs were transformed with each of the binding domain constructs and plated onto synthetic dropout medium containing10 μg/L X-α-Gal (5-bromo-4-chloro-3-indolyl-α-d-galactopyranoside) without tryptophan, leucine, and histidine. β-Galactosidase activity was assayed in the presence of X-α-Gal.

2.6. FRET-FLIM Analysis

FRET-FLIM experiment was carried out as describe previously (Bellati et al., 2016). The 5-weeks-old tobacco leaves were infiltrated with *Agrobacterium tumefaciens* strain GV3101 with desired construct and OD at 600 nm is 0.3-0.5. After 48 hours, the FRET-FLIM analysis by Leica TCS SP5 X system equipped with a 633/1.20 numeric aperture water-immersion objective lens. From the fluorescence intensity images, the decay curves were calculated per pixel and fitted with either a mono- or double-exponential decay model using the SPCImage software (Becker & Hickl; version 3.2.3.0). The mono-exponential model function was applied for donor samples with only GFP present. The double-exponential model function was used for sample containing GFP and mCherry.

2.7. SIM imaging

SIM images were taken by a 100×/NA 1.57 Plan Apochromat objective on an Elyra PS.1 platform (Zeiss, Munich, Germany) with a pco.edge 5.5 sCMOS camera

(PCO, Kelheim, Germany) according to previously published methods (Komis et al., 2014, 2015).

2.8. Fluorescent dye and drug treatment

For FM4-64 staining, vertically grown seedlings were incubated in 1/2 MS liquid containing 5 μM FM4-64 (Invitrogen, 5 mM stock in DMSO) for 5 min at room temperature. For drug treatments, four-day-old seedlings were incubated in 1/2 MS medium containing 50 μM Brefeldin A (BFA; Takáč et al., 2011), 33 μM Wortmannin (Takáč et al., 2012), 10 mM mβCD, 10 μM flg22, 10 μM MG132, or 2 μM concanamycin A for the indicated time period before observation. The stock solutions were as follows: 50 mM BFA (Sigma-Aldrich) in DMSO; 33 mM Wortmannin (Sigma-Aldrich) in DMSO; 200 mM mβCD (Sigma-Aldrich) in deionized water; 10 mM flg22 (GL Biochem [Shanghai] Ltd.) in deionized water; 10mM MG132 (Sigma-Aldrich) in deionized water; 2 mM concanamycin A (Sigma-Aldrich) in DMSO. Each treatment for confocal imaging was repeated at least three times with similar results.

2.9. Confocal microscopy

Four-day-old seedlings were mounted in 1/2 MS liquid medium and used for confocal analysis. For imaging of GFP/FM4-64, the signals were excited at 488 nm and 514 nm and emission was detected with the detector sets BP 520-550 for green signals and LP 560–640 for red signals under a Leica TCS SP5 inverted confocal microscope with a 63×oil-immersion objective. For colocalization analyses, GFP and mCherry were excited at 488 nm and 561 nm, respectively. Fluorescence emission was detected with detector sets BP 520-555 (GFP) and LP 575 (mCherry).

2.10. VA-TIRFM live imaging and data analysis

After drug treatments, four-day-old seedlings were transferred onto a glass slide with 1/2 MS medium, covered with a coverslip, and observed under a custom-built VA-TIRFM based on an Olympus IX-71 microscope equipped with a total internal reflective fluorescence illuminator and a 100×oil-immersion objective (numerical aperture of 1.45, Olympus). The 473 nm/561 nm laser line from a diode laser

(Changchun New Industries Optoelectronics Tech. Co., Changchun, China) was used to excite GFP and mCherry. The emission fluorescence signals were detected with a back-illuminated EM-CCD camera (ANDOR iXon DV8897D-CS0-VP; And or Technology, Belfast, UK) after filtering with two band-pass filters (525/545 and 609/654 nm). The gain of the EMCCD camera was set to 300 throughout all single-molecule imaging experiments; the setting was in the linear dynamic range of the EMCCD camera. Images were acquired with an exposure time of 100 ms and analyzed with Image J software (NIH).The methods used to analyze single-particle movement were described previously (MP-BRI1).

2.11. FCS analysis

FCS was performed under a Leica TCS SP5 FCS microscope equipped with a 488-nm argon laser, in-house coupled correlator, and Avalanche photodiode. The laser was focused on the plasma membrane of a GFP-Flot1 transgenic cell to detect the fluctuations in spontaneous fluorescence intensity induced by the diffusion of fluorophores into and out of the focal volume. GFP-Flot1 density was calculated as described previously (Li et al., 2011).

2.12. FRAP analysis

An FV1000MPE multiphoton laser-scanning microscope (Olympus) was used for the FRAP experiments. A rectangular region of interest was subjected to bleaching with 100% laser power at 488 nm. Fluorescence recovery was then monitored every 5 seconds. The recovery data obtained were corrected for bleaching during imaging as described (Luu et al., 2012).

2.13. Protein extraction and immunoblot analysis

Seven-day-old seedlings of transgenic GFP-Flot1 lines were treated with 50μM CHX in two tubes for 1 h, after which 100 μM MG132 was added to one tube and liquid 1/2 MS medium was added to the other tube as a control. After 3h, the seedlings were treated with 10 μM flg22. Total proteins were extracted from seedlings treated with flg22 for 0, 30, 60, and 120 min. GFP-Flot1 protein was denatured in loading buffer (62.5 mM Tris-HCl [pH 6.8], 10% [v/v] glycerol, 2% [w/v] SDS, 2.5%

[v/v]β-mercaptoethanol, 0.01% [w/v] bromophenol blue, and 1% [w/v] PMSF) at 50°C for 5min. The proteins were separated on 12% (w/v) SDS/polyacrylamide gels and transferred to a polyvinylidene fluoride membrane (Immobilon-P; Millipore) by electroblotting. Blots were developed using an ECL Advance Western Blotting Detection Kit (Amersham) according to the manufacturer's protocol. Primary antibodies and the secondary antibody were diluted in blocking solution at the following concentrations: GFP antibody at 1:3000 and secondary antibody at 1:10000; actin was used as an internal reference.

3. Results

3.1. The Flot1 amiRNAi lines exhibit defects in response to Flg22

To investigate the function of Flot1 in *Arabidopsis*, we first performed phylogenetic analysis using Clustal W and Bio Edit. This analysis showed that *Arabidopsis* flotillin proteins, including Flot1a (Flot1, Flot1a, At5g25250), Flot1b (At5g25260) and Flot2 (At5g64870), are highly conserved (Fig. 1A). For example, UPGMA analysis showed that Flot1a shares 94% amino acid sequence similarity with Flot1b and 85% similarity with Flot2 (Fig. 1B). Interestingly, the Flotillin proteins were quite conserved in higher plants (NCBI Protein Cluster CLSN2686436), so we aligned the sequences of Flot1 homologs from different plant species (Fig. 1C). Phylogenetic tree analysis revealed that Flot1 shares high sequence similarity with flotillin proteins of other plants (Fig. 1D).

To investigate the effect of changes in *Flot1* expression on plant defense responses, we used aniline blue staining to monitor callose deposition in response to flg22. As shown in Figure 2, in untreated cotyledons, no specific aniline blue signals were observed, indicating a lack of callose deposition. When treated with flg22, the *Flot1* overexpression lines showed increased callose deposition, whereas the *Flot1* amiRNA lines (ami15-5) displayed attenuated levels of callose deposition compared to control wild-type cotyledons (Fig. 2). Importantly, transformation of the *Flot1*

ami15-5 mutant with a *35S:Flot1* construct partially rescued the defects in callose deposition (Fig. 2). These results indicate that plant defense response triggered by flg22 requires Flot1.

3.2. Dynamic behavior of Flot1 particles in the plasma membrane

We also tested whether flg22 affects the dynamic behavior of Flot1 proteins in the plasma membrane. We therefore used VA-TIRFM to monitor the trajectory and range of motion of Flot1 particles in plant cells. The trajectories of Flot1 in plants treated with and without flg22 are shown in Figure 3A. In control seedlings expressing GFP-Flot1, the range of motion of GFP-Flot1 was distributed into two subpopulations: long-distance motion (39.48% of particles, 0.44 ± 0.27 μm) and short-distance motion (60.25%, 0.18 ± 0.13 μm), with distance values (μm) representing the peak of the distribution (Fig. 3B). When treated with flg22, the range of motion of GFP-Flot1 was significantly altered compared to control cells, with only 25.91% of particles showing short-distance motion. Interestingly, most GFP-Flot1 particles in cells treated with flg22 showed much longer distance motion (0.99 ± 0.13 μm), indicating that Flot1 proteins can diffuse to a relatively wide area when triggered by flg22 (Fig. 3C).

We then investigated the dynamic properties of Flot1 in more detail by calculating velocity and diffusion coefficients. Specifically, we plotted the distribution of velocity and diffusion coefficients on histograms and fitted the curves using Gaussian functions, in which the Gaussian peaks (noted as $\hat{G}$) were considered to represent the characteristic velocity and diffusion coefficients. Except the small similar $\hat{G}$ value of velocity, big $\hat{G}$ of velocity was 1.54 ± 0.02 μm/s in control seedlings (Fig. 3D), but after treatment with flg22, the big $\hat{G}$ of velocity was 1.67 ± 0.02 μm/s (Fig. 3E), indicating that the velocity of Flot1 increased in the presence of flg22. Moreover, we found that the $\hat{G}$ of diffusion coefficients was 4.57×10^{-3} $\mu m^2/s$ (SE 2.73 to $7.66 \times 10^{-3} \mu m^2/s$) and 9.12×10^{-2} $\mu m^2/s$ (SE 8.85 to 9.40×10^{-2} $\mu m^2/s$), respectively, in control seedlings (Fig. 3F). After flg22 treatment, the $\hat{G}$ of diffusion

coefficients was 6.08×10^{-3} μm^2/s (SE 4.17 to 8.87×10^{-3}μm^2/s) and 1.14×10^{-1}μm^2/s (SE 1.12 to 1.15×10^{-1}μm^2/s), respectively, representing an increase compared to control seedlings (Fig. 3G).

3.3. The oligomerization state of GFP-Flot1 in the plasma membrane

To investigate the oligomeric states of Flot1, we used yeast two-hybrid analysis to examine the physical interaction of Flot1 with itself and with Flot2. The full-length Flot1 protein was predicted to contain SPFH and flotillin domains, as determined from BLAST analysis using the NCBI website (http://blast.ncbi.nlm.nih.gov/Blast.cgi) (Fig. 4A). As shown in Fig. 4B, full-length Flot1 clearly interacted with full-length Flot1 and with Flot2. To further determine which domain is essential for the physical interactions of flotillins, we made constructs expressing the N-terminal SPFH domain (F1, amino acid residues 1–200), the intact C-terminal flotillin domain (F2, amino acid residues 201–470), and two spilt F2 (F2-1, amino acid residues 201–351; F2-2, amino acid residues 352–470) truncations. We then examined the interactions of these truncated proteins in yeast cells (Fig. 4A). Importantly, we found that F2 interacted with Flot1 and Flot2, whereas F1 did not (Fig. 4C), suggesting that the C-terminal portion (amino acids 201–470) of Flot1 is sufficient for the interaction with Flot1 and Flot2. Further analysis showed that F2-1 and F2-2 did not interact with Flot1 or Flot2 (Figs. 1), indicating that the deletion of amino acid residues 201–351 (F2-1) or 352–470 (F2-2) completely abolished the Flot1-Flot1 and Flot1-Flot2 interactions. To further verify the Flot1 can interact with Flot1, FLIM (fluorescence lifetime imaging microscopy) analyses, based on the detection of Förster resonance energy transfer (FRET), were performed by transiently expressing Flot1-GFP and Flot1-GFP /Flot1-mCherry in tobacco leaf cells. Physical interactions were assessed by GFP fast flim time. The results showed that the Flot1-GFP average fast flim time of Flot1-GFP/Flot1-mCherry decreased to 1.973 ns compared to the control 2.611 ns (Figs. 2), suggesting that Flot1-GFP and Flot1-mCherry can interact with each other.

We further observed that GFP-Flot1 fluorescent foci formed spots of variable size in cotyledon epidermal cells by SIM (Fig. 5). To investigate the partitioning of GFP-Flot1 in the plasma membrane of living cells, we analyzed time-lapse imaging of the GFP-Flot1 spots in control (Fig. 5A) and flg22-treated cells (Fig. 5B). In contrast to control cells, flg22 treatment caused the formation of linear (arrowheads) or circular (arrows) aggregates of GFP-Flot1 spots (Fig. 5B), indicating that the aggregation status of Flot1 was affected by flg22. Besides that, we also observed that the aggregation Flot1 will be disappeared with time-lapse monitoring (Fig. 5B). This demonstrated that flg22 would contribute to the endocytosis of Flot1.

3.4. Flot1 is constitutively recycled via an endocytic pathway

To determine whether the Flot1-containing dot structures were endosomal compartments, we analyzed the distribution of GFP-Flot1 fluorescent signals stained with the membrane marker FM4-64 in cotyledon epidermal cells. Most of the green intracellular GFP-Flot1 fluorescent signals colocalized with the FM4-64 signal (Fig. 6A). After treatment with Brefeldin A (BFA) to block exocytosis, GFP-Flot1 proteins accumulated in BFA compartments, where they also colocalized with FM4-64 (Fig. 6A). To rule out the possibility that the appearance of GFP-Flot1 in the intracellular vesicles was due to the presence of newly synthesized protein, we further analyzed the localization of GFP-Flot1 in the presence of the specific protein synthesis inhibitor cycloheximide (CHX). After pretreatment with CHX for 30 min, followed by BFA treatment for 60 min, the transgenic seedlings were incubated with FM4-64. We observed the colocalization of GFP-Flot1 and FM4-64 in the BFA compartments (Fig. 6A). After pretreating GFP-Flot1-expressing cotyledon cells with flg22, the number of BFA-induced aggregates derived from GFP-Flot1, which colocalized with internalized FM4-64, increased (Fig. 6A). More importantly, when treated with flg22, the number of endosomes labeled with Flot1-GFP and FM4-64 significantly increased in the cotyledon epidermal cells (Fig. 6B and 6C), suggesting that Flot1 is subject to constitutive endocytic turnover and that flg22 increases the endocytosis of GFP-Flot1.

We also used fluorescence cross spectroscopy (FCS), which allows monitoring of fluctuations in fluorescence intensity within the focal volume of the laser beam, to measure the density of GFP-Flot1 in the plasma membrane (Figs. 3A). The mean density of GFP-Flot1 was 19.4 ± 3.9 molecules μm^{-2} in control seedlings (Figs. 3B). A lower GFP-Flot1 density (14.0 ± 1.7 molecules μm^{-2}; 28% decrease with respect to control cells; $P < 0.01$, t-test) was detected after treatment with flg22 (Figs. 3B), indicating that fewer GFP-Flot1 molecules accumulated in the plasma membrane after treatment with flg22.

3.5. Flot1 is trafficked to early and late endosomal compartments

To determine the precise subcellular trafficking pathway for Flot1, we crossed plants expressing GFP-Flot1 with plants expressing the early endosome marker protein VHA-a1-mRFP; we then used the resulting plants to analyze the colocalization of GFP- and mRFP-labeled endosomes. Confocal imaging showed that GFP-Flot1 partially colocalized with VHA-a1-mRFP (Fig. 7A). We then used BFA, which resulted in the accumulation of GFP-Flot1 proteins in the BFA compartments, where it colocalized with VHA-a1-mRFP (Fig. 7A). This result indicated that Flot1 partially trafficked to early endosomes.

To further elucidate the cycling of GFP-Flot1 between intracellular compartments and the plasma membrane, we examined the dynamics of GFP-Flot1 in the plasma membranes of *Arabidopsis* cotyledon epidermal cells using fluorescence recovery after photobleaching (FRAP). The bleached regions of interest were divided into top, middle, and bottom areas and GFP signals in the three regions recovered at similar rates (Fig. 7B), suggesting that GFP-Flot1 is primarily recycled from the cytoplasm to the plasma membrane.

To investigate whether GFP-Flot1 can be transported to the prevacuolar compartment/late endosome, we crossed plants expressing GFP-Flot1 with plants expressing the prevacuolar compartment marker protein RabG3f-mRFP and SNX1-mRFP. Colocalization experiments on the resulting plants revealed

considerable overlap of GFP-Flot1 with RabG3f-mRFP (Fig. 8A) and SNX1-mRFP (Figs. 4). We then treated the plants with flg22, resulting in more colocalization of GFP-Flot1 with RabG3f-mRFP (Fig. 8B), suggesting that flg22 might increase trafficking of GFP-Flot1 to the late endosome. After pretreatment with flg22, followed by treatment with Wortmannin (an inhibitor of phosphatidylinositol-3 kinase), we determined that GFP-Flot1 was clearly induced to form rounded structures, where it colocalized with the prevacuolar compartment marker RabG3f-mRFP (Fig. 8C). The colocalization between Flot1 and RabG3f was further confirmed by quantitative analysis using the protein proximity index (PPI) (Zinchuk et al., 2011). The three-dimensional (3D) plots of the cross-correlation of GFP-Flot1 and RabG3f -mRFP were respectively shown as Figure 8D and Figure 8E. At control cells, the mean PPI values were 0.16 ± 0.03 for Flot1/RabG3f (Fig. 8F). After flg22 treatment, the mean PPI values were 0.25 ± 0.03 for Flot1/RabG3f (Fig. 8F), indicating that the trafficking of GFP-Flot1 to the late endosome was increased in response to flg22.

3.6. Proteasome-mediated degradation of GFP-Flot1

Ubiquitination leads to protein degradation or, in some cases, modulates the activity or localization of a protein (MacGurn et al., 2012). To further examine the fate of Flot1, we measured Flot1 levels before and after flg22 treatment. After pretreating the seedlings with CHX for 30 min, followed by flg22 treatment for 0, 30, 60, or 120 min, we extracted total proteins from the transgenic seedlings. Immunoblot analysis showed that the protein level of GFP-Flot1 was almost unchanged within 30 min of flg22 treatment, followed by a gradual decrease (Fig. 9A), indicating that GFP-Flot1was degraded in a time-dependent manner after treatment with flg22. Under these conditions, treatment with MG132, an inhibitor of proteasome-mediated degradation, dramatically inhibited the degradation of internalized Flot1 (Fig. 9B), suggesting the involvement of the 26S proteasome in Flot1 degradation. Moreover, we pretreated the GFP-Flot1 seedlings with 10 mM methyl-β-cyclodextrin (mβCD, which depletes sterols from the plasma membrane) for 30 min, followed by flg22 for

the indicated time periods. Immunoblot analysis showed that the degradation of Flot1 was affected by the presence of mβCD (Fig. 9), suggesting that mβCD interfered with the degradation of Flot1 when sterols were depleted, which indirectly disrupted the membrane microdomains.

4. Discussion

Plasma membranes are highly dynamic, complex structures. The dynamics of plasma membrane proteins are closely linked to many fundamental cellular processes (Shinozaki et al., 2009; Zhang et al., 2009). Therefore, studying membrane dynamics in living cells with new techniques may help decipher these complex systems (Li et al., 2013). In the present study, we used VA-TIRFM, which has an improved signal-to-noise ratio (Konopka et al., 2008; Li et al., 2011; Fan et al., 2013), to examine the dynamics of GFP-Flot1 in living cotyledon epidermal cells. In control seedlings expressing GFP-Flot1, the range of motion of GFP-Flot1 was distributed into two subpopulations. Interestingly, in cells treated with flg22, the GFP-Flot1 proteins moved over a much longer distance, indicating that activated Flot1 proteins can diffuse to relatively wide areas. Additionally, we found that GFP-Flot1 puncta at the plasma membrane had different diffusion coefficients, and Flg22 treatment increased $\hat{G}$ compared to control seedlings. These results indicate that GFP-Flot1 is highly mobile and heterogeneously distributed at the plasma membrane and that flg22 treatment increases the diffusion of Flot1, which is likely essential for activation of the immune response.

Plasma membrane proteins can also form clusters in membrane microdomains (Weisz and Rodriguez-Boulan, 2009; Hartman and Groves, 2011). Members of the stomatin/prohibitin/flotillin/HflK/C (SPFH) domain-containing protein family tend to form oligomers (Browman et al., 2007). For example, prohibitins, stomatin, and podocin form large multimeric complexes of twelve or more monomers (Langhorst et al., 2005; Tatsuta et al., 2005; Huber et al., 2006). Also, the *Arabidopsis* KAT1 K^+

channel forms punctate structures of approximately 0.5–0.6 μm on the plasma membrane (Sutter et al., 2007). Blue native-PAGE and bimolecular fluorescence complementation assays confirmed that SUT1, a sucrose transporter, forms a homodimer in the plant cell and that oxidative reagents promote its dimerization. In addition, SUT1 forms clusters with a diameter of 200–300 nm in membrane microdomains (Krügel et al., 2008). Similarly, remorin forms clusters, which are sensitive to treatment with mβCD (Raffaele et al., 2009). In the current study, yeast two-hybrid analysis demonstrated that the full-length Flot1 protein could interact with full-length Flot1 and Flot2, suggesting that the flotillin family proteins can form oligomers, as was previously demonstrated in mammals (Solis et al., 2007). Moreover, we found that GFP-Flot1 was aggregated and devoid from plasma membrane triggered by flg22, indicating that the aggregation status of GFP-Flot1 contribute to its endocytosis. Together, these results provide strong evidence that the oligomer assembly and aggregation status of Flot1 is favorable for the Flot1 associated endocytosis.

Endocytosis plays a vital role in the acquisition of materials from the extracellular space and in maintaining the protein and lipid composition of the plasma membrane (Conner and Schmid, 2003; Tanaka et al., 2009; Chen et al., 2011; Šamaj 2012). BRASSINOSTEROID INSENSITIVE1 (BRI1) localizes to the plasma membrane and endosomal structures; its localization and turnover are independent of brassinosteroids (Geldner et al., 2007). In contrast to BRI1, the plasma membrane receptor FLAGELLIN SENSING 2 (FLS2) is internalized depending on its ligand composition (Robatzek et al., 2006). The current results show that Flot1 localized to the plasma membrane and cytoplasmic compartments, and colocalized with FM4-64, suggesting that the Flot1-containing dot structures are endosomal compartments. The endocytosis of GFP-Flot1was increased in response to the flg22 treatment. Additionally, FCS analysis also showed that following flg22 pretreatment, the density of Flot1 on the plasma membrane significantly decreased in cotyledon epidermal cells. Thus, it is

reasonable to conclude that flg22 enhances the internalization of Flot1, which in turn attenuates the activated signaling in the plasma membrane.

The occurrence of endocytic trafficking in plants is well established (Barberon et al., 2011; Šamaj 2012; Fan et al., 2015). A key example is endocytosis of PIN proteins, which can enter an endocytic trafficking pathway and localize to *trans*-Golgi/early endosome compartments, followed by transport for vacuolar degradation (Petrasek et al., 2006; Kleine-Vehn and Friml, 2008; Laxmi et al., 2008). In this study, we resolved the endocytic pathway of Flot1 in the presence of flg22. Under steady state conditions, colocalization analysis showed that GFP-Flot1 partially colocalized with VHA-a1-mRFP. Importantly, FRAP analysis further suggested that GFP-Flot1 is primarily recycled from the cytoplasm to the plasma membrane. Maybe some of the recovered GFP-Flot1 comes from protein recycling between PM and cytoplasm or newly synthesized. This phenomenon is similar to AP2σ-GFP (Fan et al., 2013). But it is different from another microdomain marker protein Rem1.3, which has almost no photorecovery after photobleaching (Demir et al., 2013). VHA-a1-mRFP is an early endosomal marker (Zhang et al., 2011), indicating that Flot1 can localize in early endosomes. When treated by flg22, major Flot1 particles were internalized and tended to colocalize with RabG3f-mRFP, a late endosomal marker, thereby preventing bacterial infections. Since our results demonstrate that endocytosis of Flot1 depends on its status by flg22, our findings indicate that different regulatory mechanisms function during recycling and degradation of plasma membrane proteins, and more importantly, that internalization of Flot1 to the late endosomes/vacuoles for degradation is enhanced in response to pathogen attack. A similar observation of a regulatory switch between the recycling and degradation pathways of endocytosis was previously reported for boron exporter BOR1 (Takano et al., 2005; Kasai et al., 2011).

Ubiquitination is well-known pathway that functions in diverse cellular processes, including the regulation of endocytosis, nutrient uptake, and synaptic molecule recycling (MacGurn et al., 2012). Ubiquitination was shown to be associated with

proteasome-dependent degradation. For example, the auxin efflux carrier PIN2, the water channel aquaporin PIP2;1, and the flagellin receptor FLS2 are ubiquitinated *in vivo* (Abas et al., 2006; Lee et al., 2009; Lu et al., 2011). Recently, Martins et al. found that ubiquitination regulates BRI1 internalization and vacuolar targeting (Martins et al., 2015). In animal and yeast cells, proteasome activity interferes with protein degradation via altered targeting to the vacuole/lysosomes (van Kerkhof et al., 2001; Longva et al., 2002; Haller et al., 2014). In this study, we detected increased Flot1 degradation in a time-dependent manner after flg22 treatment. Nevertheless, the degradation of Flot1 was dramatically reduced by treatment with MG132, suggesting the involvement of the 26S proteasome in Flot1 degradation. Further biochemical and genetic studies are needed to confirm the mechanism of Flot1 ubiquitination and its role in subsequent proteasome-dependent degradation.

5. Conclusions

In summary, we showed that the dynamic and partitioning of Flot1 in plasma membrane were significantly changed when treated with the elicitor flg22 using TIRFM and SIM. Furthermore, we found that Flot1 underwent constitutive endocytic recycling pathway and that flg22 could promote endocytosis. More importantly, targeting of Flot1 to the late endosome/vacuole for degradation was increased in response to flg22. Meanwhile, immunoblot analysis showed that when triggered by flg22, GFP-Flot1 was gradually degraded in a time-dependent manner. These findings demonstrated that the dynamic and aggregation of GFP-Flot1 in plasma membrane can contribute to endocytosis and degradation of Flot1 elicited by flg22 in Arabidopsis. Our results therefore provide valuable information for further study on the molecular mechanisms underlying Flot1 involved in plant immunity.

Acknowledgements

This work was supported by the Beijing Advanced Innovation Center for Tree Breeding by Molecular Design, the Program of Introducing Talents of Discipline to Universities (111 project, B13007), the Program for Changjiang Scholars and Innovative Research Team in University (IRT13047), the National Basic Research Program of China (973 Program 2011CB809103), the National Natural Science Foundation of China (31670182, 31401149, 31530084, 31400210), and the Grant Agency of the Czech Republic (GAČR; GA16-24313S).

References

Abas, L., Benjamins, R., Malenica, N., Paciorek, T., Wisniewska, J., Moulinier-Anzola, J. C., Sieberer, T., Friml, J. and Luschnig, C., 2006. Intracellular trafficking and proteolysis of the *Arabidopsis* auxin-efflux facilitator PIN2 are involved in root gravitropism. Nat. Cell Biol. 8, 249-256.

Barberon, M., Zelazny, E., Robert, S., Conejero, G., Curie, C., Friml, J. and Vert, G., 2011. Monoubiquitin-dependent endocytosis of the iron-regulated transporter 1 (IRT1) transporter controls iron uptake in plants. Proc. Natl. Acad. Sci. USA 108, 450-458.

Bellati, J., Champeyroux, C., Hem, S., Rofidal, V., Krouk, G., Maurel, C. and Santoni, V., 2016. Novel aquaporin regulatory mechanisms revealed by interactomics. Mol. Cell Proteomics 15, 3473-3487.

Borner, G. H. H., Sherrier, D. J., Weimar, T., Michaelson, L. V., Hawkins, N. D., MacAskill, A., Napier, J. A., Beale, M. H., Lilley, K. S. and Dupree, P., 2005. Analysis of detergent-resistant membranes in *Arabidopsis*. Evidence for plasma membrane lipid rafts. Plant Physiol. 137, 104-116.

Browman, D. T., Hoegg, M. B. and Robbins, S. M., 2007. The SPFH domain-containing proteins: more than lipid raft markers. Trends Cell Biol. 17, 394-402.

Chen, X., Irani, N. G. and Friml, J., 2011. Clathrin-mediated endocytosis: the gateway into plant cells. Curr. Opin. Plant Biol. 14, 674-682.

Clough, S. J. and Bent, A. F., 1998. Floral dip: a simplified method for Agrobacterium-mediated transformation of *Arabidopsis thaliana*. Plant J. 16, 735-743.

Conner, S. D. and Schmid, S. L., 2003. Regulated portals of entry into the cell. Nature 422, 37-44.

Demir, F., Horntrich, C., Blachutzik, J., Scherzer, S., Reinders, Y., Kierszniowska, S., Schulze, W., Harms, G., Hedrich., R., Geiger, D. and Kreuzer, I. 2013. *Arabidopsis* nanodomain-delimited ABA signaling pathway regulates the anion channel SLAH3. Proc. Natl. Acad. Sci. USA 110, 8296-8301.

Fan, L., Hao, H., Xue, Y., Zhang, L., Song, K., Ding, Z., Botella, M. A., Wang, H. and Lin, J., 2013. Dynamic analysis of *Arabidopsis* AP2 σ subunit reveals a key role in clathrin-mediated endocytosis and plant development. Development 140, 3826-3837.

Fan, L., Li, R., Pan, J., Ding, Z. and Lin, J., 2015. Endocytosis and its regulation in plants. Trends Plant Sci. 20, 388-397.

Fujiwara, M., Hamada, S., Hiratsuka, M., Fukao, Y., Kawasaki, T. and Shimamoto, K., 2009. Proteome analysis of detergent-resistant membranes (DRMs) associated with OsRac1-mediated innate immunity in rice. Plant Cell Physiol. 50, 1191-1200.

Geldner, N., Anders, N., Wolters, H., Keicher, J., Kornberger, W., Muller, P., Delbarre, A., Ueda, T., Nakano, A. and Jurgens, G., 2003. The *Arabidopsis* GNOM ARF-GEF mediates endosomal recycling, auxin transport, and auxin-dependent plant growth. Cell 112, 219-230.

Geldner, N., Friml, J., Stierhof, Y. D., Jurgens, G. and Palme, K., 2001. Auxin transport inhibitors block PIN1 cycling and vesicle trafficking. Nature 413, 425-428.

Geldner, N., Hyman, D. L., Wang, X., Schumacher, K. and Chory, J., 2007. Endosomal signaling of plant steroid receptor kinase BRI1. Genes Dev. 21,1598-1602.

Glebov, O. O., Bright, N. A. and Nichols, B. J., 2006. Flotillin-1 defines a clathrin-independent endocytic pathway in mammalian cells. Nat. Cell Biol. 8, 46-U16.

Hagedorn, M. and Soldati, T., 2007. Flotillin and RacH modulate the intracellular immunity of *Dictyostelium* to *Mycobacterium marinum* infection. Cell Microbio. 9, 2716-2733.

Haller, M., Hock, A. K., Giampazolias, E., Oberst, A., Green, D. R., Debnath, J., Ryan, K. M., Vousden, K. H. and Tait, S. W., 2014. Ubiquitination and proteasomal degradation of ATG12 regulates its proapoptotic activity. Autophagy 10, 2269-2278.

Haney, C. H. and Long, S. R., 2010. Plant flotillins are required for infection by nitrogen-fixing bacteria. Proc. Natl. Acad. Sci. USA 107: 478-483.

Haney, C. H., Riely, B. K., Tricoli, D. M., Cook, D. R., Ehrhardt, D. W. and Long, S. R., 2011 Symbiotic rhizobia bacteria trigger a change in localization and dynamics of the *Medicago truncatula* receptor kinase LYK3. Plant Cell 23, 2774-2787.

Hartman, N. C. and Groves, J. T., 2011. Signaling clusters in the cell membrane. Curr. Opin. Cell Biol. 23, 370-6.

Huber, T. B., Schermer, B., Muller, R. U., Hohne, M., Bartram, M., Calixto, A., Hagmann, H., Reinhardt, C., Koos, F., Kunzelmann, K. et al., 2006. Podocin and MEC-2 bind cholesterol to regulate the activity of associated ion channels. Proc. Nat.l Acad. Sci. USA 103, 17079-17086.

Kasai, K., Takano, J., Miwa, K., Toyoda, A. and Fujiwara, T., 2011. High boron-induced ubiquitination regulates vacuolar sorting of the BOR1 borate transporter in *Arabidopsis thaliana*. J. Biol. Chem. 286, 6175-6183.

Keinath, N. F., Kierszniowska, S., Lorek, J., Bourdais, G., Kessler, S. A., Shimosato-Asano, H., Grossniklaus, U., Schulze, W. X., Robatzek, S. and Panstruga, R., 2010. PAMP (pathogen-associated molecular pattern)-induced changes in plasma membrane compartmentalization reveal novel components of plant immunity. J. Biol. Chem. 285, 39140-39149.

Kierszniowska, S., Seiwert, B. and Schulze, W. X., 2009. Definition of *Arabidopsis* sterol-rich membrane microdomains by differential treatment with methyl-beta-cyclodextrin and quantitative proteomics. Mol. Cellular Proteomics 8: 612-623.

Kim, M. G., da Cunha, L., McFall, A. J., Belkhadir, Y., DebRoy, S., Dangl, J. L. and Mackey, D., 2005. Two *Pseudomonas syringae* type III effectors inhibit RIN4-regulated basal defense in *Arabidopsis*. Cell 121, 749-759.

Kleine-Vehn, J. and Friml, J., 2008. Polar targeting and endocytic recycling in auxin-dependent plant development. Annu. Rev. Cell Dev. Biol. 24, 447-473.

Korhonen, JT., Puolakkainen, M., Häivälä, R., Penttilä, T., Haveri, A., Markkula, E., and Lahesmaa, R., 2012. Flotillin-1 (Reggie-2) contributes to *Chlamydia pneumoniae* growth and is associated with bacterial inclusion. Infect Immun. 80, 1072-1078.

Komis, G., Mistrik, M., Šamajová, O., Doskocilová, A., Ovečka, M., Illés, P., Bartec, J., Šamaj, J., 2014. Dynamics and organization of cortical microtubules as revealed by superresolution structured illumination microscopy. Plant Physiol. 165, 129-146.

Komis, G., Mistrik, M., Šamajová, O., Ovecka, M., Bartek, J., and Šamaj, J., 2015a. Superresolution live imaging of plant cells using structured illumination microscopy. Nat. Protoc. 10:1248-1263.

Komis G, Šamajová O, Ovečka M, and Šamaj, J., 2015b. Super-resolution Microscopy in Plant Cell Imaging. Trends Plant Sci. 20: 834-843.

Konopka, C. A., Backues, S. K. and Bednarek, S. Y., 2008. Dynamics of *Arabidopsis* dynamin-related protein 1C and a clathrin light chain at the plasma membrane. Plant Cell 20, 1363-1380.

Krügel, U., Veenhoff, L. M., Langbein, J., Wiederhold, E., Liesche, J., Friedrich, T., Grimm, B., Martinoia, E., Poolman, B. and Kühn, C., 2008. Transport and sorting

of the *Solanum tuberosum* sucrose transporter SUT1 is affected by posttranslational modification. Plant Cell 20, 2497-2513.

Lajoie, P. and Nabi, I. R., 2010. Lipid rafts, caveolae, and their endocytosis, Int Rev Cell Mol. Biol. *282*, 135-163.

Langhorst, M. F., Reuter, A. and Stuermer, C. A., 2005. Scaffolding microdomains and beyond: the function of reggie/flotillin proteins. Cell Mol. Life Sci. 62, 2228-2240.

Laxmi, A., Pan, J., Morsy, M. and Chen, R., 2008. Light plays an essential role in intracellular distribution of auxin efflux carrier PIN2 in *Arabidopsis thaliana*. PLoS One 3, e1510.

Lee, H. K., Cho, S. K., Son, O., Xu, Z., Hwang, I. and Kim, W. T., 2009. Drought stress-induced Rma1H1, a RING membrane-anchor E3 ubiquitin ligase homolog, regulates aquaporin levels via ubiquitination in transgenic *Arabidopsis* plants. Plant Cell 21, 622-641.

Lefebvre, B., Furt, F., Hartmann, M. A., Michaelson, L. V., Carde, J. P., Sargueil-Boiron, F., Rossignol, M., Napier, J. A., Cullimore, J., Bessoule, J. J. et al., 2007. Characterization of lipid rafts from *Medicago truncatula* root plasma membranes: A proteomic study reveals the presence of a raft-associated redox system. Plant Physiol. 144, 402-418.

Lefebvre, B., Timmers, T., Mbengue, M., Moreau, S., Herve, C., Toth, K., Bittencourt-Silvestre, J., Klaus, D., Deslandes, L., Godiard, L. et al., 2010. A remorin protein interacts with symbiotic receptors and regulates bacterial infection. Proc. Natl. Acad. Sci. USA 107, 2343-2348.

Li, R., Liu, P., Wan, Y., Chen, T., Wang, Q., Mettbach, U., Baluška, F., Šamaj, J., Fang, X. and Lucas, W. J., 2012. A membrane microdomain-associated protein, *Arabidopsis* Flot1, is involved in a clathrin-independent endocytic pathway and is required for seedling development. Plant Cell 24, 2105-2122.

Li, X., Wang, X., Yang, Y., Li, R., He, Q., Fang, X., Luu, D. T., Maurel, C. and Lin, J., 2011. Single-molecule analysis of PIP2;1 dynamics and partitioning reveals multiple modes of *Arabidopsis* plasma membrane aquaporin regulation. Plant Cell 23, 3780-3797.

Li, X. J., Luu, D. T., Maurel, C. and Lin, J. X., 2013. Probing plasma membrane dynamics at the single-molecule level. Trends Plant Sci. 18, 617-624.

Liu, P., Li, R.L., Zhang, L., Wang, Q.L., Niehaus, K., Baluška, F., Šamaj, J. and Lin J. X., 2009. Lipid microdomain polarization is required for NADPH oxidase-dependent ROS signaling in *Picea meyeri* pollen tube tip growth. Plant J. 60, 303-313.

Longva, K. E., Blystad, F. D., Stang, E., Larsen, A. M., Johannessen, L. E. and Madshus, I. H., 2002. Ubiquitination and proteasomal activity is required for transport of the EGF receptor to inner membranes of multivesicular bodies. J. Cell Biol. 156: 843-854.

Lu, D., Lin, W., Gao, X., Wu, S., Cheng, C., Avila, J., Heese, A., Devarenne, T. P., He, P. and Shan, L., 2011. Direct ubiquitination of pattern recognition receptor FLS2 attenuates plant innate immunity. Science 332, 1439-1442.

Luu, D. T., Martiniere, A., Sorieul, M., Runions, J. and Maurel, C., 2012. Fluorescence recovery after photobleaching reveals high cycling dynamics of plasma membrane aquaporins in *Arabidopsis* roots under salt stress. Plant J. 69, 894-905.

MacGurn, J. A., Hsu, P. C. and Emr, S. D., 2012. Ubiquitin and membrane protein turnover: from cradle to grave. Annu. Rev. Biochem. 81, 231-259.

Martins, S., Dohmann, E. M., Cayrel, A., Johnson, A., Fischer, W., Pojer, F., Satiat-Jeunemaitre, B., Jaillais, Y., Chory, J., Geldner, N. et al., 2015. Internalization and vacuolar targeting of the brassinosteroid hormone receptor BRI1 are regulated by ubiquitination. Nat. Commun. 6: 6151.

Morel, J., Claverol, S., Mongrand, S., Furt, F., Fromentin, J., Bessoule, J. J., Blein, J. P. and Simon-Plas, F., 2006. Proteomics of plant detergent-resistant membranes. Mol. Cell Proteomics 5, 1396-1411.

Ovečka, M., Berson, T., Beck, M., Derksen, J., Šamaj, J., Baluska, F. and Lichtscheidl, I.K., 2010. Structural sterols are involved in both the initiation and tip growth of root hairs in *Arabidopsis thaliana*. Plant Cell 22, 2999-3019.

Perraki, A., Cacas, J. L., Crowet, J. M., Lins, L., Castroviejo, M., German-Retana, S., Mongrand, S. and Raffaele, S., 2012. Plasma membrane localization of *Solanum tuberosum* remorin from group 1, homolog 3 is mediated by conformational changes in a novel C-terminal anchor and required for the restriction of *potato virus X* movement. Plant Physiol.160, 624-637.

Petrasek, J., Mravec, J., Bouchard, R., Blakeslee, J. J., Abas, M., Seifertova, D., Wisniewska, J., Tadele, Z., Kubes, M., Covanova, M. et al., 2006. PIN proteins perform a rate-limiting function in cellular auxin efflux. Science 312, 914-918.

Raffaele, S., Bayer, E., Lafarge, D., Cluzet, S., German Retana, S., Boubekeur, T., Leborgne-Castel, N., Carde, J. P., Lherminier, J., Noirot, E. et al., 2009. Remorin, a *solanaceae* protein resident in membrane rafts and plasmodesmata, impairs *potato virus X* movement. Plant Cell 21, 1541-1555.

Robatzek, S., Chinchilla, D. and Boller, T., 2006. Ligand-induced endocytosis of the pattern recognition receptor FLS2 in *Arabidopsis*. Genes Dev. 20, 537-42.

Shahollari, B., Peskan-Berghofer, T. and Oelmuller, R., 2004. Receptor kinases with leucine-rich repeats are enriched in Triton X-100 insoluble plasma membrane microdomains from plants. Physiol. Plant 122, 397-403.

Shi, H., Guo, G., Liu, R., Wang, C., Xu, X. and Ruan, L. 2016. Membrane associated protein flotillin-2 in Litopenaeus vannamei plays a role in WSSV infection. Fish Shellfish Immunol. 54, 247-253.

Shinozaki, Y., Sumitomo, K., Tsuda, M., Koizumi, S., Inoue, K. and Torimitsu, K., 2009. Direct observation of ATP-induced conformational changes in single P2X(4) receptors. PLoS Biol. 7, e1000103.

Simon-Plas, F., Perraki, A., Bayer, E., Gerbeau-Pissot, P. and Mongrand, S., 2011. An update on plant membrane rafts. Curr. Opin. Plant Biol. 14, 642-649.

Simons, K. and Gerl, M. J., 2010. Revitalizing membrane rafts: new tools and insights. Nat. Rev. Mol. Cell Biol. 11, 688-699.

Simons, K. and Toomre, D., 2000. Lipid rafts and signal transduction. Nat. Rev. Mol. Cell Bio. 1, 31-39.

Solis, G. P., Hoegg, M., Munderloh, C., Schrock, Y., Malaga-Trillo, E., Rivera-Milla, E. and Stuerivier, C. A. O., 2007. Reggie/flotillin proteins are organized into stable tetramers in membrane microdomains. Biochem. J. 403, 313-322.

Stanislas, T., Bouyssie, D., Rossignol, M., Vesa, S., Fromentin, J., Morel, J., Pichereaux, C., Monsarrat, B. and Simon-Plas, F., 2009. Quantitative proteomics reveals a dynamic association of proteins to detergent-resistant membranes upon elicitor signaling in tobacco. Mol. Cell Proteomics 8, 2186-2198.

Šamaj J., 2012. Endocytosis in Plants. ISBN 978-3-642-32462-8, Springer, Berlin, Heidelberg, pp. 336.

Sutter, J. U., Sieben, C., Hartel, A., Eisenach, C., Thiel, G. and Blatt, M. R., 2007. Abscisic acid triggers the endocytosis of the *Arabidopsis* KAT1 K^+ channel and its recycling to the plasma membrane. Curr. Biol. 17, 1396-1402.

Takáč, T., Pechan, T., Richter, H., Müller, J., Eck, C., Böhm, N., Obert, B., Ren, H., Niehaus, K and Šamaj J., 2011, Proteomics on brefeldin A-treated Arabidopsis roots reveals profilin 2 as a new protein involved in the cross-talk between vesicular trafficking and the actin cytoskeleton. J. Proteome Res. 10: 488-501.

Takáč, T., Pechan, T., Šamajová, O., Ovečka, M., Richter, H., Eck, C., Niehaus, K. and Šamaj, J., 2012. Wortmannin treatment induces changes in Arabidopsis root proteome and post-Golgi compartments. J. Proteome Res. 11: 3127-3142.

Takano, J., Miwa, K., Yuan, L., von Wiren, N. and Fujiwara, T., 2005. Endocytosis and degradation of BOR1, a boron transporter of *Arabidopsis thaliana*, regulated by boron availability. Proc. Natl. Acad. Sci. USA 102, 12276-12281.

Tanaka, H., Kitakura, S., De Rycke, R., De Groodt, R. and Friml, J., 2009. Fluorescence imaging-based screen identifies ARF GEF component of early endosomal trafficking. Curr. Biol. 19, 391-397.

Tatsuta, T., Model, K. and Langer, T., 2005. Formation of membrane-bound ring complexes by prohibitins in mitochondria. Mol. Biol. Cell 16, 248-259.

van Kerkhof, P., Alves dos Santos, C. M., Sachse, M., Klumperman, J., Bu, G. and Strous, G. J., 2001. Proteasome inhibitors block a late step in lysosomal transport of selected membrane but not soluble proteins. Mol. Biol. Cell 12, 2556-2566.

Wan, Y., Ash, W. M., 3rd, Fan, L., Hao, H., Kim, M. K. and Lin, J., 2011. Variable-angle total internal reflection fluorescence microscopy of intact cells of *Arabidopsis thaliana*. Plant Methods 7, 27.

Weisz, O. A. and Rodriguez-Boulan, E., 2009. Apical trafficking in epithelial cells: signals, clusters and motors. J. Cell. Sci. 122, 4253-4566.

Zhang, L., Zhang, H., Liu, P., Hao, H., Jin, J. B. and Lin, J., 2011. *Arabidopsis* R-SNARE proteins VAMP721 and VAMP722 are required for cell plate formation. PLoS One 6, e26129.

Zhang, Q., Li, Y. and Tsien, R. W., 2009. The dynamic control of kiss-and-run and vesicular reuse probed with single nanoparticles. Science 323, 1448-1453.

Figure Legends

Fig. 1. Phylogenetic analysis of Flotillin proteins in *Arabidopsis* and angiosperms. (A) Sequence alignment of Flotillin family proteins (Flot1a, Flot1b, Flot2) from *Arabidopsis* using Clustal W and BioEdit. The red-shaded amino acids indicate identical sites and the green-shaded amino acids indicate similar sites. (B) UPGMA analysis of flotillin proteins in *Arabidopsis* based on genetic distance. (C) Sequence alignment of FLOT homologs from different species using ClustalW and Bioedit. The red shaded zones are identical sites, the green shaded zones are similar sites, and the threshold for shading are above 90%. (D) Phylogenetic tree of the FLOT homolog proteins in angiosperms. The aligned sequences were used to construct MP tree and BI tree using Paup 4.0 b10 and MrBayes3.1.2. Numbers above branches indicate bootstrap values for the MP analyses and Bayesian posterior probabilities, respectively.

Fig. 2. Detection of callose deposition in *Arabidopsis* cotyledon cells. (A) The magnification images of callose deposition in OE, WT, ami15-5 and COM cotyledons cells. (B) Quantification of callose deposition in OE, WT, ami15-5 and COM cotyledons cells. **P<0.01, Student's t-test. Scale bar: 100 μm.

Fig. 3. Dynamic behavior of individual GFP-Flot1 spots imaged with VA-TIRFM in *Arabidopsis* cotyledon epidermal cells. (A) Time-lapse trajectories of GFP-Flot1 at different time points (0, 3.5, 7.0 and 10.5 s) for control (upper panels) and flg22-treated cotyledon epidermal cells (lower panels) in *Arabidopsis*. (B) Motion range of GFP-Flot1 in *Arabidopsis* cotyledon epidermal cells (control; n = 1670 spots). (C) Motion range of GFP-Flot1 in *Arabidopsis* cotyledon epidermal cells after treatment with flg22 (n = 1462 spots). (D) Distribution of GFP-Flot1 velocity on the cotyledon epidermal cell plasma membrane (n = 3544 spots). (E) Distribution of GFP-Flot1 velocity on the cotyledon epidermal cell plasma membrane in the presence

of flg22 (n = 8952 spots). (F) Distribution of GFP-Flot1 diffusion coefficients on the cotyledon epidermal cell plasma membrane (n = 3577 spots). (G) Distribution of GFP-Flot1 diffusion coefficients on the cotyledon epidermal cell plasma membrane in the presence of flg22 (n = 4109 spots). Scale bars: 2 μm.

Fig. 4. Yeast two-hybrid assay of Flot1 and Flot1/Flot2. (A) Schematic representation of full-length Flot1 and deletion constructs. F1 indicates the N-terminal SPFH_flotillin domain and F2 indicates the C-terminal flotillin domains, which are divided into F2-1 and F2-2. (B) Yeast two-hybrid analyses of the interactions between Flot1 and Flot1/Flot2. Full-length Flot1 and full-length Flot2 were fused to the GAL4 DNA-binding domain (BD) and the GAL4 activation domain (AD). (C) Yeast two-hybrid assay of the interaction of Flot1 domains with Flot1/Flot2. Full-length Flot1 was fragmented into F1 and F2, which were separately fused to the GAL4 activation domain (AD).

Fig. 5. Structured illumination microscopy (SIM) live imaging of Flot1 distribution in plasma membrane. (A) Flot1 particles showed reduced mobility in control cells. (B) Formation of Flot1 aggregates (arrowheads) and Flot1 devoid from membrane domains (arrows) during flg22 treatment. Numbers in top right corner correspond to elapsed time in seconds. Scale bars: A: 10 μm; B: 5 μm.

Fig. 6. Confocal images showing localization of GFP-Flot1 in transgenic *Arabidopsis* lines. (A) Cotyledon epidermal cells were stained with FM4-64 and the colocalization of GFP-Flot1 and FM4-64 was observed at the plasma membrane and in intracellular structures (white arrow). When cotyledon epidermal cells were pretreated with BFA (50μM) for 1 h, followed by incubation with FM4-64 for 30 min, GFP-Flot1 colocalized with FM4-64 in the BFA compartments. Arrows indicate BFA bodies.

When cotyledon epidermal cells were pretreated with CHX (50 μM) for 30 min, followed by pre-incubation in BFA (50 μM) for 1 h before staining with FM4-64 for an additional 30 min, colocalization of GFP-Flot1 and FM4-64 was observed in the BFA compartment (white arrow). When cotyledon epidermal cells were pretreated with flg22 (10 μM) for 60 min, followed by pre-incubation in BFA (50 μM) for 1 h before staining with FM4-64 for an additional 30 min, GFP-Flot1 colocalized with FM4-64 was observed in the BFA compartment (white arrow). For all analyses, the results shown are representative of >15 independent samples. GFP-Flot1 (green), FM4-64 labeling (red), merged channels (yellow). (B) In control cotyledon epidermal cells, colocalization of GFP-Flot1 and FM4-64 was observed at the plasma membrane and the intracellular structures (upper panels, white arrowheads). When cotyledon epidermal cells were pretreated with flg22 for 1 h and incubated with FM4-64 for 30 min, GFP-Flot1 colocalized with FM4-64 (lower panels, white arrowheads). (C) Quantification of endosomes/cell in control and flg22-treated cells. For all analyses, the results shown are representative of >15 independent samples. **P<0.01, Student's t-test. Scale bars: 20 μm.

Fig. 7. Flot1 partially colocalizes with early endosomal markers. (A) GFP-Flot1 colocalized with VHA-a1-mRFP endosomal markers in crossed transgenic lines. White arrows indicate endosomes showing colocalization. GFP-Flot1 is shown in green, VHA-a1-mRFP in red, and the merged image indicates colocalization (yellow). When cotyledon epidermal cells were pretreated with BFA (50 μM) for 1 h, GFP-Flot1 co-localized with VHA-a1-mRFP in the BFA compartment (white arrows). (B) Fluorescence recovery curves represent the best fits from 20 cells. Error bars indicate s.d. The initial bleached region was subdivided into three areas, as indicated by red, green, and blue rectangles. Scale bars: 20 μm.

Fig. 8. Flot1 partially colocalizes with late endosomal markers. (A) GFP-Flot1 colocalized with RabG3f-mRFP endosomal markers in crossed transgenic lines. Arrows indicate endosomes showing colocalization. GFP-Flot1 is shown in green, RabG3f-mRFP in red, and the merged image indicating colocalization (yellow). (B) When cotyledon epidermal cells were treated with flg22 (10 μM) for 30 min. GFP-Flot1 colocalized with RabG3f-mRFP was observed in the endosome (white arrow). (C) When cotyledon epidermal cells were pretreated with flg22 (10 μM) for 30 min, followed by a pre-incubation in Wortmannin (33 μM) for 1 h, GFP-Flot1 colocalized with RabG3f-mRFP in small vacuoles (white arrows). (D) 3D plot of GFP-Flot1 and RabG3f-mRFP cross-correlation versus pixel shift. (E) 3D plot of GFP-Flot1 and RabG3f-mRFP cross-correlation versus pixel shift after flg22 treatment. (F) Mean protein proximity index values (*n*=10 images from 10 cells). **P<0.01, Student's t-test. Scale bars: 20 μm.

Fig. 9. Degradation of Flot1 after flg22 treatment. (A) Total proteins were isolated from GFP-Flot1 seedlings that had been treated with flg22, with or without MG132 or mβCD, in the presence of CHX for 0, 30, 60, or 120 min. The total proteins were separated by SDS-PAGE and immune detected with GFP antibody. (B) Relative contents of GFP-Flot1 (per unit of total protein). Error bars represent standard errors. The protein level of 0 min was set to 100, and the relative protein levels of the other treated plants were obtained.

Figures

Fig. 1

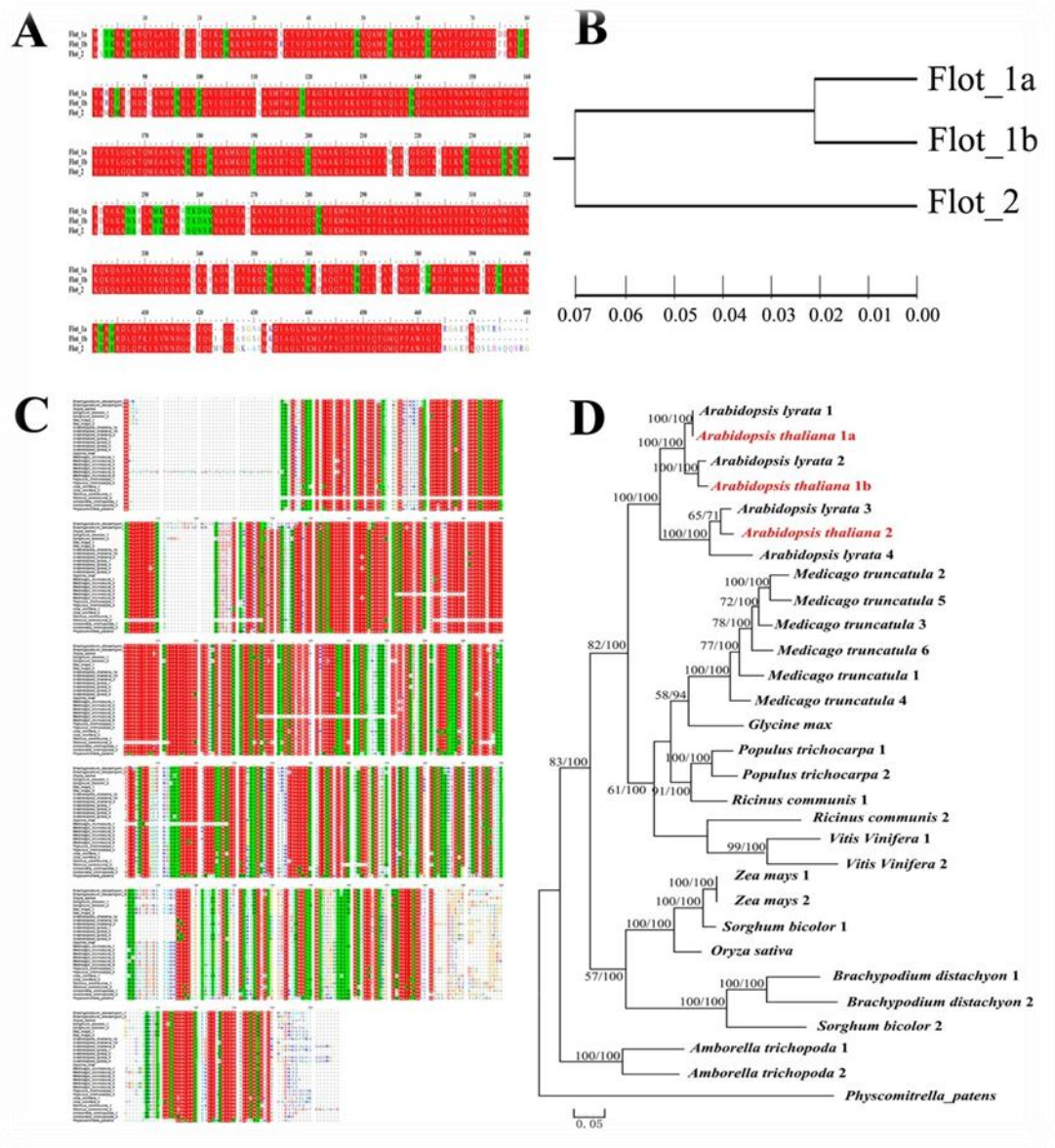

Fig. 2

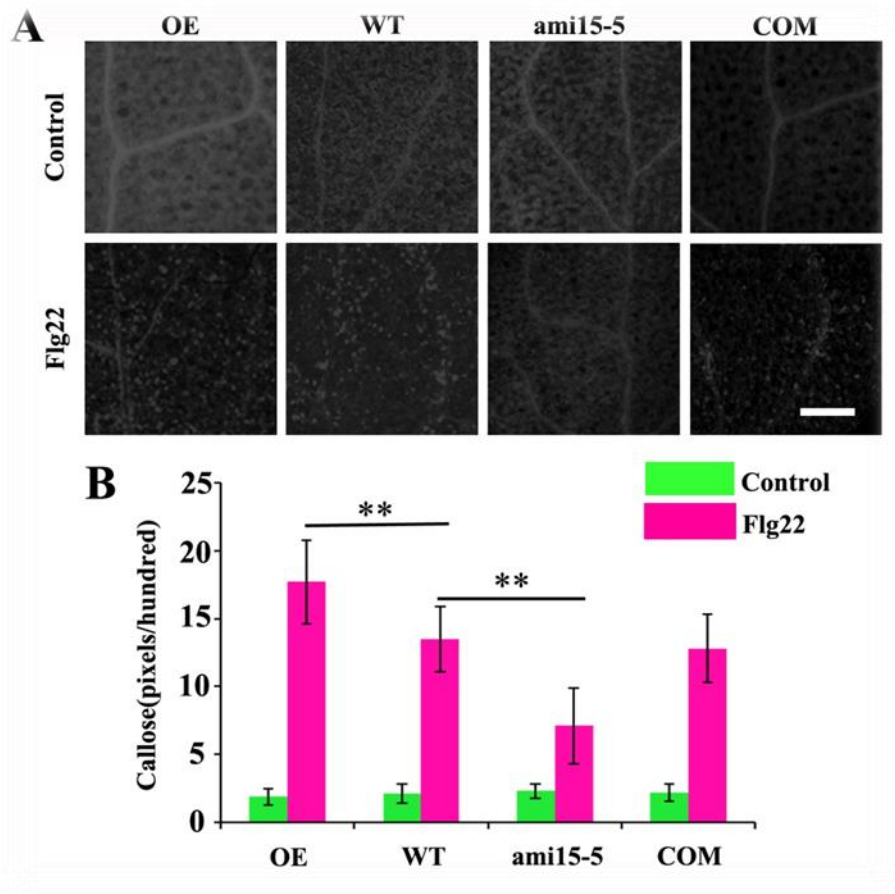

Figure 3

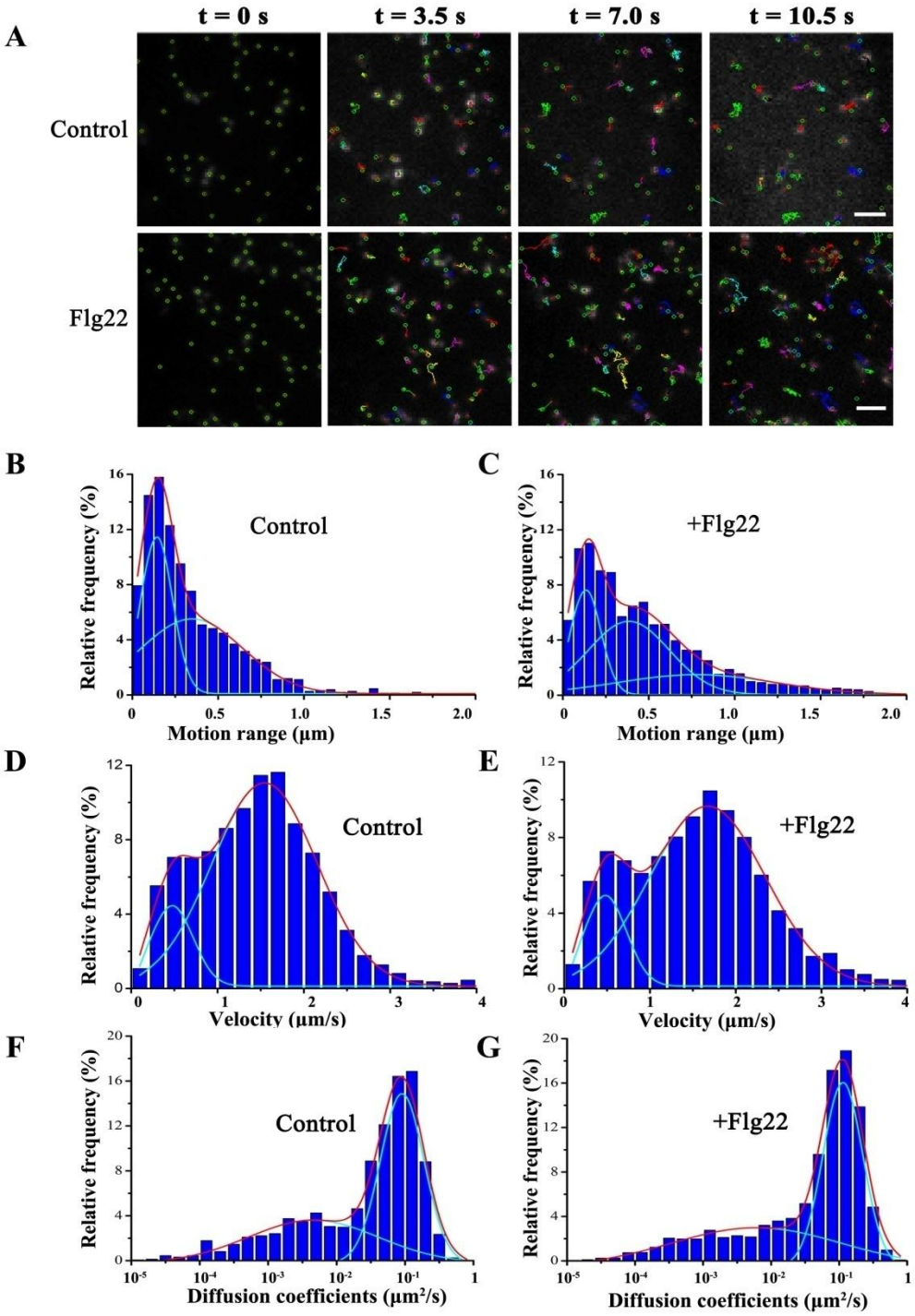

Fig. 4

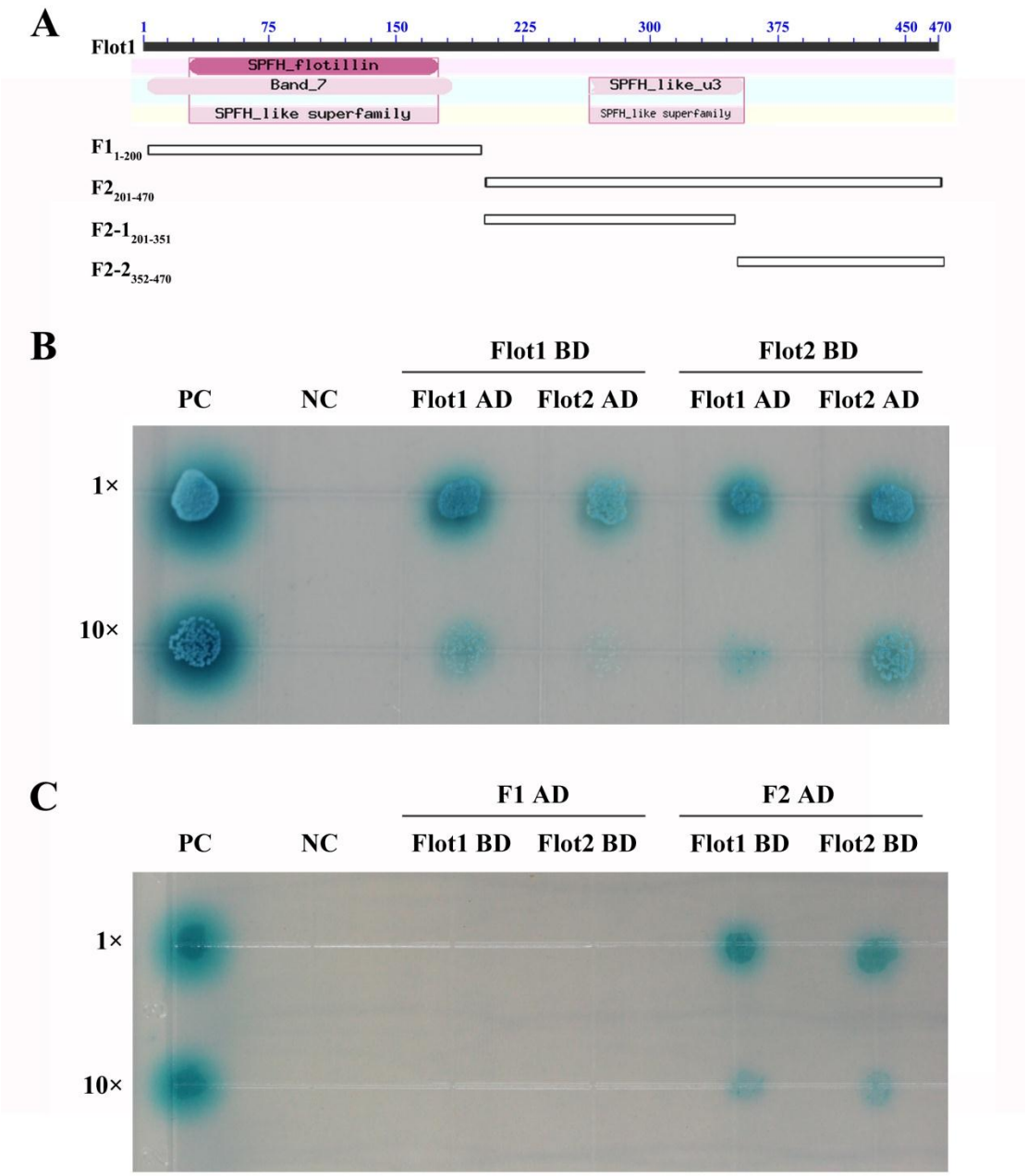

Fig. 5

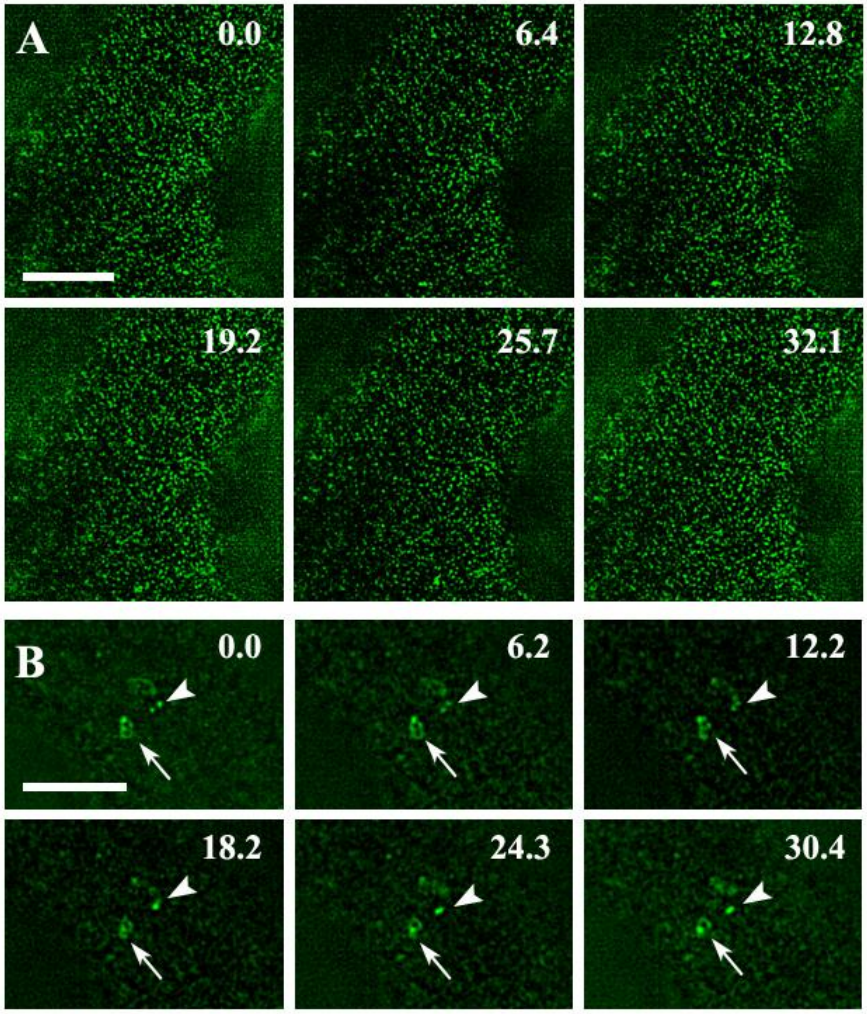

Fig. 6

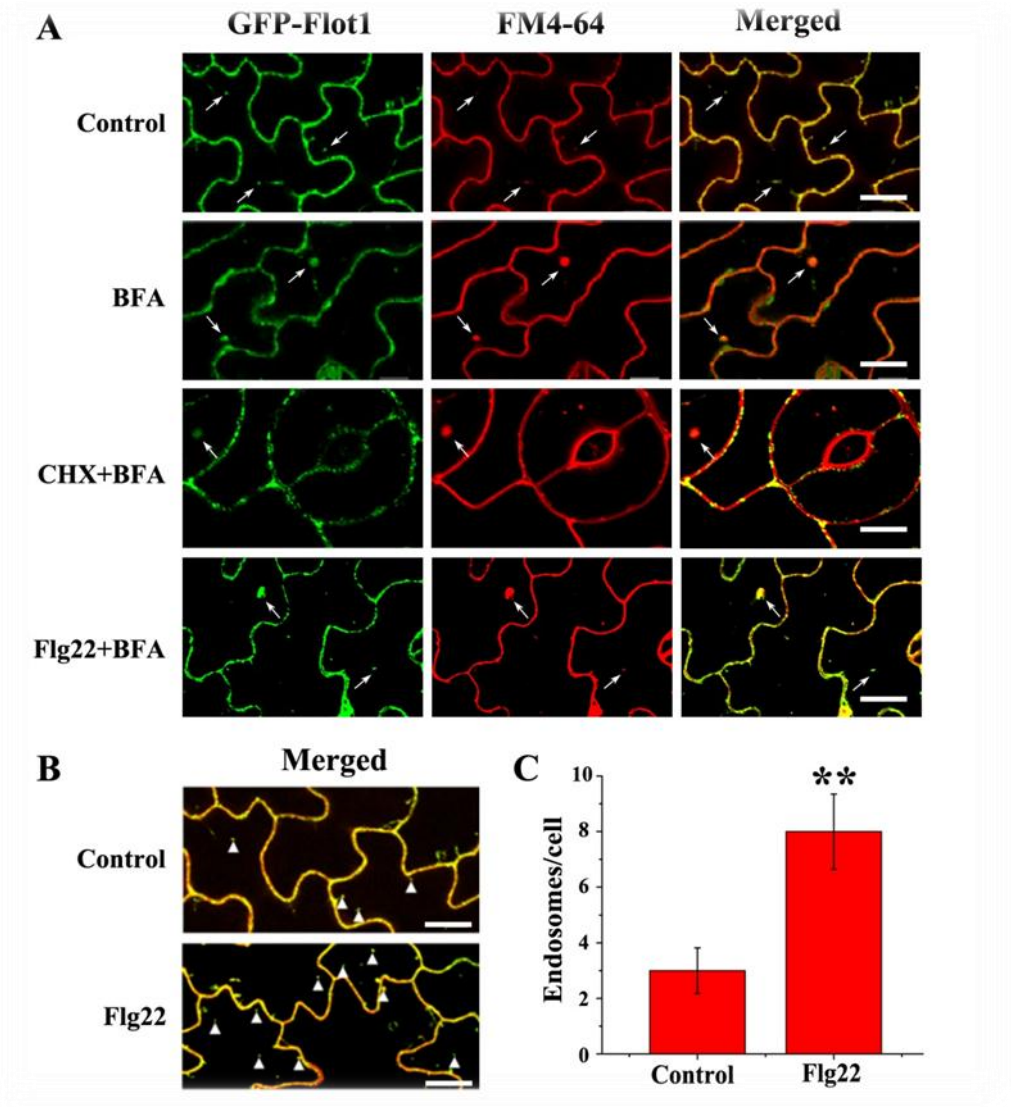

Fig. 7

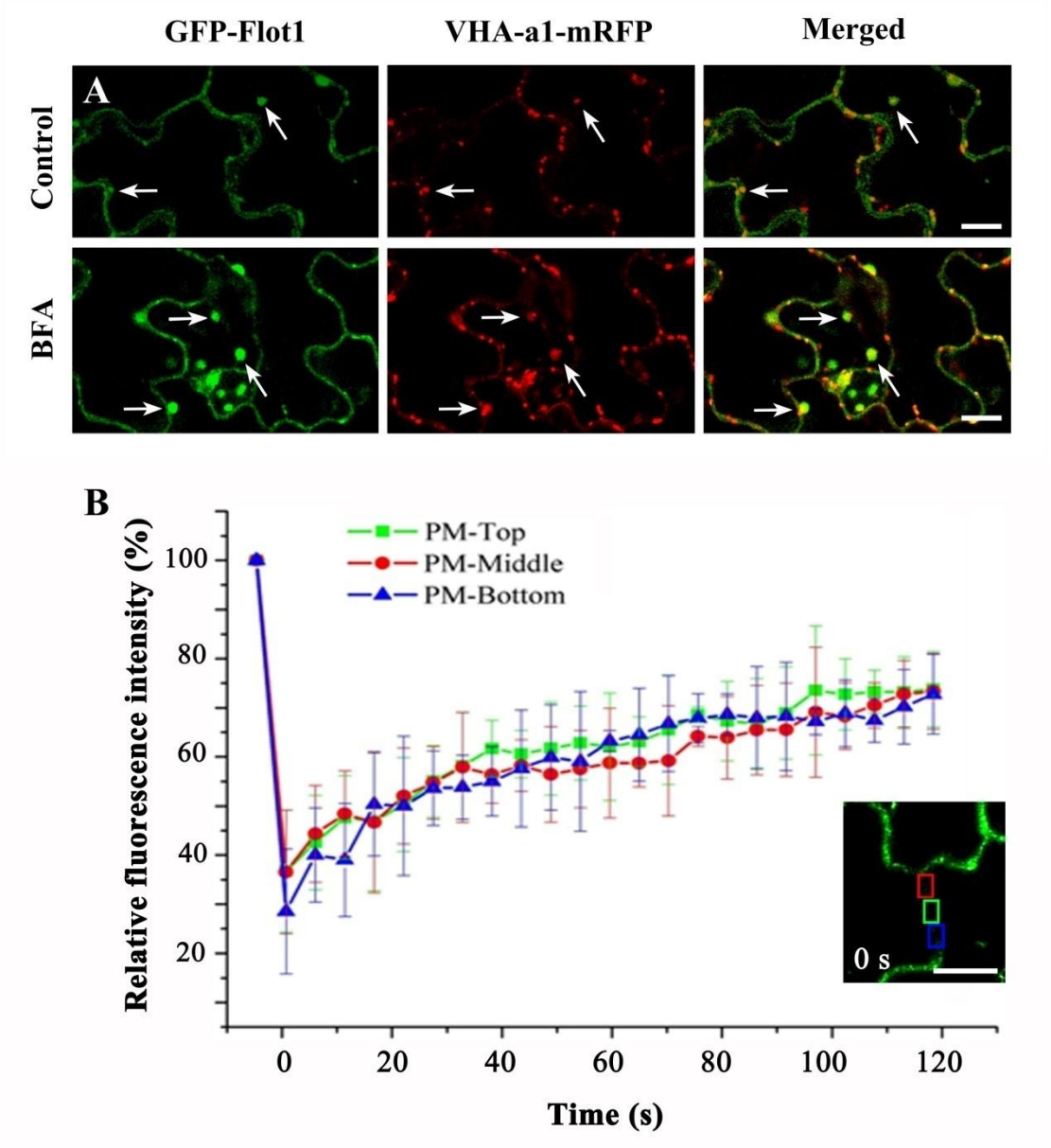

Fig. 8

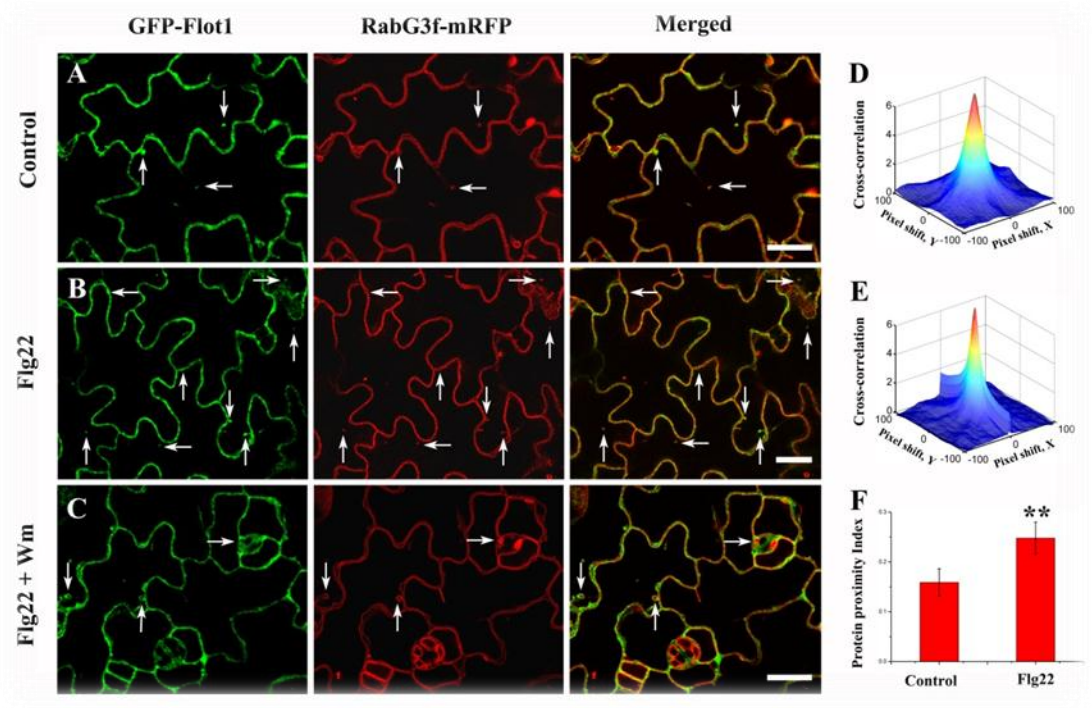

Fig. 9